Session IX. Airborne Passive Infrared

N91-24147

Status of Colorado State Universities' IR Research
Dr. Pete Sinclair, Colorado State University

An Airborne FLIR Detection and Warning System for Low Altitude Wind Shear

Peter C. Sinclair
Department of Atmospheric Science
Colorado State University
Fort Collins, CO

Peter M. Kuhn
ARIS, Inc.
Fort Collins, CO

October 18, 1990

To be published in:

The Journal of Applied Meteorology
November 1990

Abstract

There is now considerable evidence to substantiate the causal relationship between low altitude wind shear (LAWS) and the recent increase in low-altitude aircraft accidents. The National Research Council (1983) has found that for the period 1964 to 1982, LAWS was involved in nearly all the weather related air carrier fatalities. However, at present, there is no acceptable method, technique, or hardware system that provides the necessary safety margins, for spatial and timely detection of LAWS from an aircraft during the critical phases of landing and takeoff. The Federal Aviation Administration (FAA) has addressed this matter (Federal Registry, 1988) and supports the development of an airborne system for detecting hazardous LAWS with at least a one minute warning of the potential hazard to the pilot. One of the purposes of this paper is to show from some of our preliminary flight measurement research that a forward looking infrared radiometer (FLIR) system can be used to successfully detect the cool downdraft of downbursts (microbursts/macrobursts) and thunderstorm gust front outflows that are responsible for most of the LAWS events. The FLIR system provides a much greater safety margin for the pilot than that provided by reactive designs such as inertial-air speed systems that require the actual penetration of the MB before a pilot warning can be initiated. Our preliminary results indicate that an advanced airborne FLIR system could provide the pilot with remote indication of MB threat, location, movement, and predicted MB hazards along the flight path ahead of the aircraft.

In a proof-of-concept experiment, we have flight tested a prototype FLIR system (non-scanning, fixed range) near and within Colorado MB's with excellent detectability. The results show that a minimum warning time of one-four minutes (5-10 km), depending on aircraft speed, is available to the pilot prior to MB encounter. Analysis of the flight data with respect to a modified 'Hazard Index' indicates the severe hazard that the apparently weak and innocuous MB's present to both the commercial transport pilots as well as the much larger number of pilots who fly the smaller general aviation and executive aircraft.

1. Introduction

Over the past few years the importance of low altitude wind shear (LAWS) from thunderstorm outflows and downbursts to aviation safety has resulted in the development of several new detection techniques and warning systems. The driving force for this atmospheric research had its roots in the sobering statistics of LAWS related accidents. The 1975 Eastern Airlines accident at Kennedy Airport (Fujita, 1985) provided much of the impetus for this initial research and development work.

The National Transportation Safety Board (NTSB) statistics show that 1987 was the worst year for air travel since 1974 with 31 aircraft accidents claiming 231 lives. A number of these accidents were related to low altitude wind shear (LAWS)[1] incidents during the approach or takeoff phases. In addition, a study conducted by the National Research Council (1983) for the period 1964 to 1982 showed that LAWS was involved in nearly all the air carrier fatalities. Since 1982, the NTSB has studied three additional LAWS accidents, including the widely publicized Delta Airline microburst accident at Dallas/Fort Worth International Airport where 134 passengers and crew were killed. These studies do not include similar statistics for the largest aircraft segment of the country, i.e. private and executive aircraft or general aviation aircraft (GA). Because of their low-altitude operating regime GA aircraft have increased possibilities of encountering dangerous wind shear events. Aircraft with high airspeed and wind loading appear to be more sensitive to head/tail wind variations than aircraft with low airspeed and wing loading which are more sensitive to downdraft/updraft penetrations (Stengel, 1984). Our preliminary studies suggest that many small, private aircraft accidents, especially over high terrain are the result of LAWS generated by gust fronts (GF), and/or micro-macroburst (MB) activity.

Although, significant progress has been made in the development and testing of the TDWR[2] and the LLWAS[3] for large airport LAWS hazards (Mahoney, *et al.* 1989; Turnbull.

[1]LAWS as used in this proposal is a generic term which includes the wind shear/vertical motion fields produced by gust fronts (GF), and microbursts/macrobursts (MB).
[2]TDWR: Terminal Doppler Weather Radar (Research Applications Program, 1988)
[3]LLWAS: Low Level Windshear Alert System (Wilson and Flueck, 1986; Goff and Gramzow, 1989)

et al., 1989; Goff and Gramzow, 1989; McCarthy and Wilson, 1985; Campbell, *et al.*, 1989; Smythe, 1989), the FAA (Federal Registry, 1988) and other Federal agencies now recognizes that there is a need for an airborne low altitude wind shear system that will:

1. supplement the planned 47 airport deployment of LLWAS and TDWR warning systems, and

2. provide an on-board aircraft system that will indicate low altitude wind shear hazards at all airports for all commercial aircraft during the critical landing and takeoff phases.

The importance of an airborne system is manifested in its unique capability to search, in real-time, the airspace directly ahead of the aircraft for suspected LAWS/MB activity during the entire approach to or departure from all runways at any airport. Figure 1 schematically depicts a possible LAWS/MB scenario for the landing (LDG) and takeoff (T/O) phases that involve a MB penetration. The foward looking infrared radiometer (FLIR) system remotely monitors the cold downdraft region of the MB vertical core as the aircraft descends along the glide slope toward the runway. Prior to and during takeoff, the aircraft FLIR system can scan vertically and horizontally ahead of the aircraft to detect MB activity. Airborne inertial systems must first sense positive deviations above the glide slope due to an increase in headwinds or vertical motions (R_{L_1}) before corrective action can be initiated (Fig. 1). Further penetration into the MB to R_{L_2} are needed by these reactive systems to completely assess the MB intensity and safety of flight. A similar situation develops for aircraft departures through a MB at locations R_{T_1} and R_{T_2}. It is well recognized that severe MB wind fields are capable of bringing down any commercial or private aircraft now flying. Consequently, aircraft inertial systems do not provide adequate warning for avoidance or escape of severe LAWS/MB situations. Even in nonsevere situations they do not provide avoidance capability and may be marginal in providing a timely alert to the pilot and/or flight control system. In essence they are a reactive not a predictive flight safety system.

2. The Forward-Looking Infrared Radiometer (FLIR) System

a. Instrumentation

Our objective has been to determine the applicability of a prototype infrared (IR) system for airborne, advance detection of thunderstorm downbursts which lead to low altitude wind shear (Fig. 2). The IR sensing system is a precision radiation thermometer with an instantaneous field of view (IFOV) of 2 deg. and special filters for sensing in the 13 to 15 micrometer portion of the atmospheric molecular spectrum of CO_2. The radiometer is mounted (forward pointing) under the wing of a small atmospheric research aircraft (Fig. 3). The wing suspension strut and instrument pod for the radiometer are located such that the radiometer IFOV is outside the propellor arc.

A highly efficient onboard data acquisition system provides the data processing and calculation of Doppler winds, gust gradient observations (3-axis gust probe system) together with all standard meteorological parameters (Sinclair and Purdom, 1989, 1983). An advanced, high accuracy DME/LORAN-C navigation system allows precise positioning of the aircraft with respect to the location of advance shear detection and subsequent shear encounter. The central processing unit (MASSCOMP multi-bus computer) provides data sampling (25–100 samples sec^{-1}), storage, calculation, and graphical display in quasi-real-time. All data sampled is initially stored on hard disk (80 megabytes) and then it is dumped to a compact, cassette type tape for final storage prior to landing. Post flight data processing is accomplished on the airborne computer and then dumped to a printer/graphics ground system. During the research flight the computer also provides current graphical display of all the parameters for real-time display and control of the flight operations.

b. Atmospheric Physics of Microburst Detection

Previous work by several authors has shown that there is a demonstrated relationship between the temperature difference across a shear-producing gust front or downburst outflow and the wind speed and direction of the gust front outflow. The larger temperature differences appear to produce higher wind shear or peak gusts. Fawbush and Miller (1954),

Foster (1958), and Proctor (1989) have provided a physical basis for predicting surface peak gusts caused by thunderstorm density currents. Temperature drops of 5°C may readily accompany peak gusts of 17 m s^{-1} while those of 15°C are associated with peak gusts of approximately 40 m s^{-1} (Fig. 4). The more recent work by Proctor (1989) involving MB modeling tends to corroborate these earlier results of Fawbush and Miller and Foster for non-frontal thunderstorms. For example, Proctor's results show a maximum deviation from earlier data of approximately −4 m s^{-1} at a temperature drop (ΔT) of approximately 6°C. At other ΔT values the surface wind gust values are also slightly lower with both data sets indicating nearly identical peak winds at ΔT = 16°C.

On the other hand, however, Fujita (1985) has shown that 40% of NIMROD and JAWS microbursts are warmer than their enviroment at the surface. The outflow is then not strictly analogous to a relatively cold gravity or density current, although it initially may have a similar momentum structure. As a result, the temperature anomaly across the leading edge of the outflow at the surface may not always indicate a cool gravity current outflow with a known temperature drop vs. maximum wind gust relationship. Thus, a FLIR temperature sensing-wind shear predictor system that looks at the surface outflow region would give confusing results much of the time. In addition, infrared observations of the surface outflow during the landing approach would also include a ground surface heat source term that would swamp the MB outflow signal. Consequently, our present FLIR system has an IFOV that intercepts the MB in a horizontal plane (Fig. 1). Thus, as the aircraft descends, successively lower regions of the MB vertical core are remotely sensed by the FLIR system. Below approximately 300 m AGL, the FLIR system will at some point intercept the MB outflow region. However, the FLIR system is designed to provide a warning signal to the pilot long before this low altitude-low speed situation develops. Consequently, the FLIR detected temperature anomalies will normally not include those positive anomalies that may be measured in the surface layer. If positive temperature anomalies exist significantly above the surface layer, then the MB will in all probability not be a flight hazard.

In some of our previous research [Kuhn *et al.* (1983), Kuhn and Sinclair (1987), Sinclair and Kuhn (1989)] low level penetrations of downbursts and microbursts indicated that the magnitude of the time rate of change of temperature difference ($\frac{\Delta T}{\Delta t}$) was indicative of gust front intensity. These results suggested that the criterion for potential shear warning was $-0.5°C/s$. For larger negative values of $\frac{\Delta T}{\Delta t}$, the algorithm applied to the radiometer output predicts gust front shear to also increase. Note we are continuing our FLIR measurements in order to increase the number of MB penetrations from which statistical and dynamical formulations can be developed between the MB temperature anomaly and the low altitude wind shear intensity.

In a horizontally uniform temperature field, both the near filter channel of the radiometer, or the static air temperature measured at the aircraft, and the forward, long-range sensing filter channel of the radiometer sense the same temperature. As a cool MB is approached, the long range channel begins to sense a cooler temperature well before the aircraft reaches the gust front, and the near channel senses the warmer static temperature at the aircraft until the cool downdraft or gust front is penetrated (Fig. 1). At this point both radiometers sense the same temperature for a period of time. No alert for LAWS is produced until the temperature difference between the forward sensed temperature and the aircraft temperature reaches the predetermined negative threshold (ΔT) and/or negative rate threshold ($\frac{\Delta T}{\Delta t}$).

The width of the FLIR radiometer filter pass band, $\Delta\nu$, is an important consideration in designing the optics of the FLIR LAWS radiometer (Caracena, *et al.*, 1981). Theoretical considerations show that narrow pass bands give the best spatial discrimination of thermal perturbations, while broad pass bands produce the strongest corresponding perturbation signal in the radiometer output.

Radiation in the atmospheric molecular spectrum of carbon dioxide (N_E) and from the target (N_T) that reaches the radiometer optics detector may be expressed as

$$N = N_E + N_T[\text{watts cm}^{-2}\text{sr}^{-1}]$$

or

$$N = \int_{\nu}\int_{x} B(\nu,T)\phi(\nu)\left(\frac{\partial\tau_{\Delta\nu}(u[CO_2])}{\partial x}\right)dxd\nu + \int_{\nu} B(\nu,T_o)\phi(\nu)\tau_o(\nu)d\nu \qquad (1)$$

See Appendix 1 for explanation of symbols. The first term in Eq. (1) represents emitted radiance from the atmosphere (well-mixed CO_2) while the second term represents the target radiance transmitted through the atmosphere to the detector.

In the first term (N_E) of Eq. (1) the horizontal transmission may be expressed as

$$\tau_{\Delta\nu} = exp(-k_{\Delta\nu}q\rho x) \qquad (2)$$

where the product, $q\rho$, is the mean density of carbon dioxide gas. The weighting function distance in Eq. (1) is given by $\frac{\partial\tau_{\Delta\nu}}{\partial x}$ as a function of the horizontal path distance, x. Equation (2) may be differentiated with respect to distance, x, to give the logarithmic weighting function:

$$\frac{\partial\tau}{\partial \ln x} = \frac{\partial\tau}{\partial x}x = -k_{\Delta\nu}q\rho\tau x \qquad (3)$$

This term weights the radiance received from the target at the radiometer from distance increments in the direction of the target, such as a cold microburst or gust front where LAWS may exist. This weighting function thus characterizes the contribution of IR radiation in the wavelength range selected by the filter through portions of the atmosphere along the cone of acceptance of the IR sensor. The choice of the filter spectral band (determined by the cut-on and cut-off filter wavelengths) therefore determines the range or 'look distance' of the radiometer. The 'look distance' (L) is defined as the weighted mean distance ($\bar{x}$), i.e.

$$L \equiv \bar{x} = \frac{\int_o^\infty \frac{\partial\tau}{\partial x}x dx}{\int_o^\infty \frac{\partial\tau}{\partial x}dx} \qquad (4)$$

A detailed evaluation of Eq. (3) as a function of various horizontal distances, x, and altitudes (33 to 800 m) over various pass bands at 10 cm^{-1} intervals in the 667 to 710 cm^{-1} (14.99–14.08 μm) portion of the CO_2 spectrum (Fig. 5) provides a large matrix of logarithmic weighting functions. For our prototype IR detector system, we selected a weighting function centered near 700 cm^{-1} (14.29 μm) which results in a theoretical, fixed 'look-distance' of approximately 5.0 km (Fig. 6). This configuration would give approximately 100–140

seconds warning time to microburst and shear encounter for our aircraft penetration speeds. For transport aircraft which have approach speeds of approximately 150 mph, the warning time to MB penetration would be only slightly less, i.e. 75–105 seconds.

The second term (N_T) in Eq. (1) represents the target temperature which in this case refers to the cool downdraft or microburst at temperature (T_o). If the target is at or within the equivalent 'look distance', it will be easily detected. For targets beyond the 'look distance', the atmospheric transmittance [$\tau(\Delta\nu)$] will act to suppress the target radiance. The technique is to scan radially (in combination with azimuth scanning) with various filters [$\phi(\nu)$] until a particular 'look distance' provides a maximum change in radiance. This provides an estimate of the target distance from the FLIR system.

c. FLIR System Performance

To establish some confidence in the ability of the FLIR system to detect MB temperature anomalies of at least a few degrees centigrade, an analysis of the detection system noise equivalent radiance (NEN) and noise equivalent temperature difference (NEΔT) thresholds was accomplished. The FLIR system employs a hyperimmersed thermister bolometer detector in the front end of a precision radiation thermometer which has the following specifications:

$\omega \equiv$ solid angle intercept at detector, $[\Delta\phi(1 - \cos\Delta\theta)]$; sr^{-1}
$\Delta\theta, \Delta\phi \equiv$ detector IFOV, (2.0°); where θ and ϕ are spherical coordinates
$\Delta f \equiv$ electronic bandwidth (1.0 Hz)
$T_f \equiv$ filter efficiency (0.68)
$T_l \equiv$ lens efficiency (0.44)
$k_e \equiv$ electronic system noise factor (1.2)
$A_o \equiv$ optics clear aperature (0.785 cm^2)
$A \equiv$ detector area ($0.25 \times 10^{-4} cm^2$)
$D^* \equiv$ detector detectivity (3.0×10^8cm $Hz^{1/2}W^{-1}$)

From these system parameters the noise equivalent radiance (NEN) can be calculated,

$$NEN = \frac{\sqrt{A}\sqrt{\Delta f}k_e}{D^* A_o w T_f T_l}$$

or

$$NEN = 4.0 \times 10^{-6} \text{watts cm}^{-2}\text{sr}^{-1}.$$

The NEN provides a lower threshold at which the FLIR system can detect atmospheric radiant anomalies.

In terms of temperature thresholds, a compatible noise equivalent temperature difference (NETD) can also be obtained from the following expression:

$$NETD = \frac{\pi F \sqrt{\Delta f n}}{(\Delta\theta) A_o \varepsilon \int_{\lambda_1}^{\lambda_2} \tau_a(\lambda)\tau_o(\lambda) D^*(\lambda) \left[\frac{\partial B(\nu, T_o)}{\partial T}\right]_{T_B} d\lambda}$$

where:

ε	≡	emissivity (1.0)
F	≡	sensor focal length (14 mm)
B	≡	Planck radiation law
T_o	≡	blackbody target temperature (292 K)
T_B	≡	background temperature (294 K)
τ_a	≡	atmospheric transmission (0.35)
τ_o	≡	optical transmission (0.30)

With these values of the system parameters, the noise equivalent temperature difference is:

$$NETD = 0.03\,K\ .$$

This NETD represents the necessary temperature difference between the MB target (292 K) and the environment (294 K) to produce a signal-to-noise ratio of unity (laboratory case, $\tau_a = 1.0$). For a real atmosphere with 350 ppm CO_2, 5 gm Kgm^{-1} water vapor, and the MB at a range of approximately 5 km, the NETD becomes:

$$NETD = 0.12\,K\ .$$

These results are compatible with the experimentally determined FLIR system sensitivity of ±0.1° K and accuracy of ±0.5° K.

These performance parameters will be improved significantly in a second generation FLIR design which employs a cooled, HgCdTe (Mercury-Cadmium-Telluride) detector that provides a NEN = 4.72×10^{-8} watts $cm^{-2}sr^{-1}$.

Atmospheric effects (absorbtion and scattering) act to degrade the FLIR system performance. We have assumed that the MB is essentially a black body radiating through an intervening FASCODE2 model atmosphere (Clough *et al.*, 1986) that absorbs (CO_2 and water vapor) and re-radiates as a black body. Background radiation is neglected since the MB

lateral and vertical dimensions provides an essentially opaque (black) body that completely intercepts the IFOV of the FLIR system. Scattering by dry atmospheric aerosols is small compared to carbon dioxide and water vapor absorbtion. For example, the LOWTRAN 7 tropospheric aerosol model (Kneizys, *et al.*, 1988) for a mid-latitude MB situation indicates that neglect of aerosol scattering leads to a percentage error that is less than 0.2%.

This analysis of the FLIR system performance provided a quantitative foundation from which we concluded that MB's with at least a ΔT = 1°–2°C could be detected remotely through an absorbing atmosphere in the 12–15 μm infrared spectral passband. The results of several relatively 'weak' (ΔT = 2°C) MB penetrations also support the results of this system analysis and show that the FLIR system estimated accuracy of ±0.5°C is met or exceeded.

We have tested this basic concept under actual flight conditions and some of these measurement results are discussed in the following sections.

3. Preliminary Measurements and Observations

a. Verification of FLIR Detectability

The prototype FLIR radiometer was installed on the right wing of our atmospheric research aircraft, a Cessna T207. A highly efficient on-board data acquisition system (MASSCOMP computer) provides digital recording (25–50 sps) of doppler winds, 3 axis gust probe and strap-down gyro parameters, along with standard meteorological parameters (Sinclair and Purdom, 1989, 1984, 1983a,b; Sinclair, 1979, 1973).

Several flight tests of our present proof-of-concept system not only brought to light several new features of the microburst phenomena but provided, as well, a real microburst environment for preliminary testing of the forward-looking IR (FLIR) wind shear detection system (Sinclair and Kuhn, 1987, 1989). Two examples of these penetrations are discussed below in order to show the potential for further development of the present proof-of-concept detection system. The approach to the microburst penetration is depicted in Fig. 7 with the winds (V_H, w), the temperature difference (ΔT_s) between the microburst and the aircraft

environment, and the FLIR temperature difference (ΔT_R) shown in Figs. 8 and 10. In these two MB penetrations the aircraft was flown in a constant attitude, constant power configuration which allowed altitude changes above and below the initial point. We believe these to be the first airborne measurements made near and within a microburst of vertical motion (w), horizontal wind (V_H), ΔT_s, and ΔT_R.

The important features of these penetrations are outlined below:

1) MB#1

(a) The penetration was begun at 1800 ft (549 m) AGL, 18 km south of the Cheyenne Ridge (Colorado-Wyoming border) on 11 August 1987 at approximately 1400 MST. The aircraft's true heading was approximately 270° at a true airspeed of 56 m sec^{-1}. The MB depiction in Fig. 7 is a reasonable facsimile of the penetration configuration. The four graphs in Fig. 8 represent (1) the atmospheric vertical motion (w) in m s^{-1}, (2) the horizontal wind (V_H) in degrees from true north (vertical lines) and knots, (3) the static (environmental) temperature (T_s) at the aircraft, and (4) the far field radiometric temperature minus the static temperature (T_s) measured at the aircraft (ΔT_R). The abcissa is the horizontal distance in kilometers from the initial point.

(b) The vertical motion field (w) shows the characteristic upward velocity of 1 m s^{-1} below the cloud on approach to the MB. The core of the MB occurs at approximately 10.0 km and is 'buried' within a heavy precipitation (HP) core (Fig. 9) where the maximum vertical velocity of $w = -12.5$ m s^{-1} is reached. A secondary region of large vertical motion ($w = -8$ m s^{-1}) was also encountered in light precipitation (LP) prior to entering the MB core at $x \approx 7.5$ km. This secondary downdraft core is driven by the upstream flow field of the downstream vortex (Fig. 9). It is important to note that this secondary downdraft core was encountered primarily because of the selected aircraft penetration altitude and heading relative to the MB orientation. Other aircraft penetration headings

and altitudes could have produced quite different secondary, as well as primary, downdraft structure due to the MB asymmetry and vortex circulation structure.

(c) The horizontal wind field (V_H) during most of the penetration indicates a headwind component of approximately 10 knots. Within the HP core of the MB the wind changes abruptly to a tailwind of 15–20 knots. This wind reversal (ΔV_H = 25–30 knots), coupled with the severe downdraft of the MB, provides a critical flight regime for aircraft maneuvering near the ground. Since this was a mid-level MB penetration (i.e. initially above the vortex flow field), the V_H wind field did not exhibit the classical strong headwind-tailwind sequence that is normally observed closer to the ground in the MB outflow region.

(d) The static temperature (T_s) measured at the aircraft represents the temperature variations near and within the MB with respect to a reference altitude ($z \approx 550$ m AGL), i.e. the initial altitude at $z = 0$. The process lapse rate required to reference the measured temperature from altitudes above and below this reference altitude was obtained from multi-level aircraft soundings near and within the MB. The temperature measurements indicate a sharp decrease at approximately $x \approx$ 5.5 km, just prior to entering the light precipitation (LP), Fig. 9. A maximum temperature deficit or change of $\Delta T_s \approx 2°C$ occurs near the backside (upstream) of the MB core just outside of the HP in the rain-cooled region.

(e) The FLIR, ΔT_R data plot indicates a target acquisition at about 3.3 km or approximately ~~8.0~~ 6.0 km from the target which represents the rain-cooled core of the wet MB at $x \approx$ ~~11.3~~ 9-10 km. As pointed out above in the temperature (T_s) discussion, the maximum ΔT_s actually occurs on the upstream or backside of the MB. However, the FLIR measured ΔT_R of –2°C agrees with the in-situ ΔT_s of –2°C, and therefore a warning of impending MB penetration of ~~at least~~ 2–3 minutes is available to the pilot of a jet transport type aircraft in the landing phase. At slower approach speeds, this warning time is significantly increased. It is important to note also, that because of the FLIR systems minimum de-

tectability of approximately ±0.5°C, the first significant temperature decrease at $x \approx 5.5$ km of $\Delta T_s = 0.5$°C, was actually detected at approximately $x \approx 1.3$ km. Consequently, this rain cooled region of the LP region which proceeded the main core of the MB, may provide alert alarms prior to penetration of the MB core on particular aircraft penetration tracks. In any case, these preliminary measurements indicate that our FLIR system can detect the MB core through light precipitation.

The cross-over point where $\Delta T > 0$ does not mean that the wet MB is now warmer than the near field static temperature. What has happened is that some of the precipitation has been deposited on the radiometer optics. This water coating on the lens has resulted in the blockage of outside radiation to the detector. The detector then also views reflected energy from the heated black body reference cavity during this part of the chopper cycle. This results in an erroneously high temperature output which will eventually approach the 45°C cavity reference. Hence, the ΔT's will progressively increase in a positive direction as indicated for ≥ 5.7 km. We are testing several design modifications which will eliminate this precipitation contamination of the FLIR optics.

2) MB#2

On the same day, a second MB penetration was made over flat terrain just north of Fort Collins, CO (Figs. 10 and 11). The important features of this penetration are outlined below:

(a) The penetration was started at 1150 ft (350 m) AGL at approximately 1500 MST. The aircraft true heading was 200° at a true airspeed of 57 m sec^{-1}. This MB configuration is similar to that depicted in Fig. 7, but with very little vortex roll-up of the outflow near the ground. The three graphs depict the same parameters as displayed in the first MB penetration (Fig. 8).

(b) The vertical motion field (w) in this case is primarily downward on approach to the wet MB. This is a result of the light rain encountered between x = 2.5 km and 5.0 km. The core of the wet MB is located at approximately 9.0 km and is 'buried' within the moderate precipitation (MP) core where the downward vertical motion reaches a maximum of $w \approx -14$ m s^{-1}. In this case, MB#2 had a much more extensive area of LP prior to penetration of the MB core which was approximately the same diameter as that of MB#1 (Figs. 9 and 11). Although the largest vertical motion ($w \approx -14$ m s^{-1}) was encountered within the MB core, the downward vertical motion was still strong just upstream from the MP in the rain-cooled region (Fig. 11). This region of downward motion appears to frequently occur on the upstream side, which appears to be a rain cooled region following the primary precipitation core of the MB.

(c) The horizontal wind field (V_H) during most of the penetration indicates a headwind component of approximately 10 knots. In this case, the wind begins to change within the core of the wet MB from southwesterly to a 5–10 knot northerly flow. While the effective headwind-tailwind component amounts to approximately 20–25 knots, the change takes place over a horizontal distance of 4–5 km. This change is more gradual in headwind-tailwind component ($\frac{\Delta V_H}{\Delta x} \approx 2.8 \times 10^{-3}$ sec^{-1}) than in MB#1 where essentially the same change occurred over a 1 km distance ($\frac{\Delta V_H}{\Delta x} \approx 13.8 \times 10^{-3}$ sec^{-1}). Note, that the shear ($\frac{\Delta V_H}{\Delta x}$) in MB#1 significantly exceeds the presently accepted minimum wind shear hazard of 2.5 x 10^{-3} sec^{-1} (Mahoney, *et al.*, 1989). Again, however, this is a mid-level MB penetration where the V_H wind field did not exhibit the classical headwind-tailwind sequence that is normally observed closer to the ground in the MB outflow regions.

(d) The temperature minimum of approximately 18.5°C occurs at x = 9.3 km (Fig. 10) which agrees well with the location of the maximum downward vertical motion of $w = -14$ m s^{-1} (Fig. 11). Thus, the total temperature deficit is approximately $\Delta T_v = 1.8$°C. The T_v measurements indicate that the cool MB downdraft

core begins at $x \approx 8.3$ km and extends to $x \approx 11.0$ km. Note, that the temperature returns slowly to a near constant environmental value of $T_s \approx 20.0°C$. This slow return of the temperature to a somewhat lower value on the upstream side of the MB is due primarily to the effect of the rain cooled region left in the 'wake' of the MB. Also, as in MB#1, there is a definite temperature decrease as the aircraft approaches or enters the precipitation regions. In MB#2, this initial temperature decrease occurs at $x \approx 5.2$ km while in MB#1 this same initial decrease of temperature occurs at $x \approx 5.5$ km. In both cases, this initial temperature decrease is associated with the approach to or encountering light precipitation (LP) preceding (or downstream of) the MB core. Penetration tracks from the upwind side of the MB would show a more gradual temperature decrease characteristic of the trailing 'wake' or rain-cooled region. On the other hand, cross-stream penetrations of the MB core may show neither of these temperature variations, especially in the case of asymmetric MB flow structure. Under particular conditions therefore, these temperature decreases may prove to be important precursors of MB presence and intensity further along the flight path. Numerical simulations of microbursts also indicate a temperature drop prior to penetration of the MB core, primarily during the increasing headwind portion of the penetration (Babcock and Droegemeier, 1989; Droegemeier and Babcock, 1989). This is easily explained in that in these cases the modeled penetration track is through the symmetrical outflow vortex roll-up which represents cooler air than the environment. However, as Proctor (1989) and others (Bedard and LeFebvre, 1986) have pointed out, the presence of a surface stable layer or warm boundary layer can greatly modify the temperature of the outflow (vortex) air—to the point, in some cases, where the increasing headwind may be warmer than the surrounding environment. In the two cases we have cited here the initial penetration flight track is just above the outflow and consequently the first temperature decrease is due to the LP region preceding the MB core.

(e) The FLIR, ΔT_R data plot suggests a MB target acquisition at $x \approx 3.0$ km or approximately 6.3 km from the MB core at $x \approx 9.3$ km (Fig. 10). In this case, the detail of the maximum ΔT_R is somewhat obscurred by the effect of the precipitation on the PRT-5 optics. In this case, the maximum temperature deficit ($\Delta T_s \approx 1.8°C$) also compares favorably with the maximum FLIR measurement of $\Delta T_R \approx 1.8°$-$2.0°C$. Again, a warning time of approximately 2 minutes is available for transport type aircraft and up to 4 minutes for smaller, general aviation aircraft. Furthermore, we believe that the MB was, in essence, initially detected at $x \approx 1.0$ km due to the cool downdraft in LP at $x \approx 5.2$ km. As in MB#1, this early detection of the cool downdraft preceding the MB core along this penetration track provides 1 minute plus alert signal at $x \approx 1.0$ km in addition to the 2 minute warning at $x \approx 5.0$ km of impending MB penetration.

b. Microburst Features Important to Flight Safety

1) Headwind/Tailwind—Vertical Motion Factor

Our flight research indicates, in agreement with previous events and research, that the low level penetration of a fully developed microburst (MB), which combines the effects of strong headwind/tailwind and vertical motion factors, can be very hazardous to the untrained pilot. However, this is not the only hazardous situation for the unsuspecting pilot. There are many more MB's that appear weak and innocuous to the pilot than there are those that can be easily distinguished by a trained pilot. Many of these so-called innocuous MB's are dry and therefore not easily detected by the proposed airport radars. However, these MB's are capable of producing vertical and horizontal flow fields that are still hazardous with respect to transport type aircraft landing and takeoff performance margins. Furthermore, pilots of smaller aircraft may well find that their aircraft landing/takeoff performance margins (climb rate, controllability, speed control, etc.) are significantly exceeded during these MB penetrations.

Consequently, in order to fully document this flight safety hazard, it is imperative that in-situ flight measurements by research aircraft be continued in a full range of MB types, at various altitudes and penetration headings with respect to the MB track. Our preliminary flight results indicate that in certain MB approach headings and altitudes the vertical motion field may provide a more hazardous flight regime than the headwind/tailwind factor. In other approach headings and MB configurations, the reverse may be true or both factors may be of near equal importance. The availability of in-situ measurements of this type by research aircraft will provide the air-truth needed for radar algorithm improvement, numerical modeling studies, and realistic aircraft simulation operation and training.

2) The Hazard Index

In order to put some of our preliminary measurements in perspective with the anticipated hazards of MB penetration, the hazard index (F) developed by Targ and Bowles (1988) is shown in Figs. 9 and 11, i.e.,

$$F = \frac{\dot{u}}{g} - \frac{w}{V}$$

along with a second hazard factor proposed by the authors,

$$F^* = F\left[1 + \frac{120\ m}{A}\right]$$

where:

$\dot{u}$ $\equiv$ Lagrangian change in the wind along the aircraft flight path
g $\equiv$ acceleration of gravity
w $\equiv$ vertical wind velocity component
V $\equiv$ true airspeed of the aircraft
A $\equiv$ altitude above ground level (AGL)

Positive values of F indicate aircraft performance loss (i.e. decreasing headwind or increasing tailwind and/or downdraft) while negative values of F indicate aircraft performance gain (i.e. increasing headwind or decreasing tailwind and/or updraft). The F factor is quantitatively related to the effect of wind shear/vertical motion on the aircraft energy state and the available rate of climb potential. We suggest an

additional hazard index factor (F^*) which is represented by the second hazard index graph (Δ) in Figs. 9 and 11. It includes the additional hazard of the aircraft AGL altitude, i.e. the potential MB hazard is substantially increased for a low level aircraft penetration *vs* one at a higher altitude where recovery may be more probable. From our experience with general aviation aircraft, an altitude loss of 250–300 m is not unusual in our present penetration technique, i.e. constant attitude–constant power profile. Note, this altitude loss results in a maximum 7–10 degree flight path angle with the horizontal and thus does not significantly affect the hazard index (F) derivation approximations. As the aircraft approaches the ground due to aircraft performance loss within the MB ($F > 0$), the hazard index (F^*) increases significantly due to the altitude term ($1 + \frac{120\,m}{A}$). Thus, F^* is always greater than F depending on the aircraft altitude (AGL). For example, at critical altitudes below 120 m, F^* will be more than twice the value of F. An analysis of a wide range of commercial aircraft (light-to-medium weight) performance capabilities indicates that the hazard index factor (F^*) could be used to alert the pilot of the flight hazards of MB penetration, i.e.

MB Flight Hazards

No hazard:	$F^* < 0.10$
Yellow alert:	$0.10 \leq F^* < 0.20$
Red alert:	$F^* \geq 0.20$

The yellow alert implies considerable caution must be exercised by the pilot to avoid unacceptable altitude/airspeed losses during MB penetration. The red alert indicates that MB penetration is not advised and appropriate abort and go-around procedures will be necessary. Consequently, in both MB#1 and MB#2 (Figs. 9 and 11), the hazard index [F or F^*] becomes significant (yellow and red alerts) from near the forward edge of the MB to an area just upstream of the rear precipitation boundary. This hazard region is generated primarily by the vertical motion term ($\frac{w}{V}$) and the ground proximity term ($1 + \frac{120\,m}{A}$). Only near the rear boundary of MB#1 (Fig. 9) does the wind shear term ($\frac{\dot{v}}{g}$) become more significant (at $x \approx 10.9$ km) than

the vertical motion term ($\frac{w}{V}$). The general dominance of the term $\frac{w}{V}$ is important when one considers that most private-commercial aircraft have easily generated climb capabilities significantly less than the 8–15 m s^{-1} vertical motions measured in MB#1 and MB#2.

4. Conclusions

We anticipate that continued aircraft probing of microbursts of various sizes and intensities at different altitudes and relative penetration headings will yield significant information on MB structure and aircraft hazards [F, F^*]. This information coupled with the FLIR (ΔT_R) measurements will provide a data base from which alert and warning algorithms can be developed for second and third generation FLIR detection systems. These on-going and future studies will bring into sharper focus the importance of water vapor absorbtion, precipitation screening of MB infrared signals, and warm MB false alarms. The latter factor, warm MB's, is considered by many to be simply a manifestation of the disturbance of the warm, surface layer air by the MB outflow. As a result, ground surface temperature measurements could indicate a warm MB core which in reality may still be colder than its environment at an altitude of 50–100 m. This warm surface layer is usually below the FLIR scan volume and would therefore not become a false alarm factor. Additional measurements will provide a clearer and quantitative picture of the actual atmospheric processes responsible for the warm MB structure.

Acknowledgements. The research was supported by NSF Grant #ATM-84-20980 (Thunderstorm Outflow Studies), NOAA Grant #43-RANR-5-03966, and ARIS, Inc., Fort Collins, CO. The authors thank Becky Armstrong for preparation of the text and Judy Sorbie-Dunn for drafting the figures.

Appendix: Symbol and Acronym Table

N, B	radiance, w cm^{-2} sr^{-1} ($B \equiv$ blackbody radiance)
K	temperature, degrees Kelvin
$k_{\Delta\nu}$	CO_2 absorption coefficient, $cm^2 g^{-1}$
q	mass mixing ratio of CO_2, g g^{-1}
T	atmospheric temperature, K
T_o	Target temperature, K (Downburst volume)
u	optical thickness of CO_2 gas (g cm^{-2})
w	vertical motion, m s^{-1}
x	horizontal distance, km
z	vertical distance, m
ΔT_R	temperature difference between FLIR sensed air temperature and the aircraft static temperature
$\frac{\Delta T_R}{\Delta t}$	time rate of change of forward looking IR air temperature minus static air temperature at aircraft, °C s^{-1}
ΔT_s	static temperature deficit between aircraft and microburst
$\Delta\nu$	optical filter band width, cm^{-1}
sr^{-1}	steradian
ν	wave number, cm^{-1}
λ	wavelength
τ	CO_2 transmittance, %
ρ	air density, g cm^{-3}, p/RT
$\phi(\nu)$	radiometer filter transmission, %
AGL	Above Ground Level
DME/LORAN-C	Distance Measuring System/Long Range Navigation System
IFOV	Instantaneous Field of View

References

Babcock, M.R. and K.K. Droegemeier, 1989: Numerical simulation of microbursts: aircraft trajectory studies, Preprints, *Third International Conference on the Aviation Weather System*, Anaheim, CA, AMS, Boston, Jan 30–Feb 3.

Bedard, A.J., Jr. and T.J. LeFebvre, 1986: Surface measurements of gust fronts and microbursts during the JAWS project: statistical results and implications for wind shear detection, prediction, and modeling, NOAA Tech. Memo. ERL WPL-135, Wave Propagation Laboratory, Boulder, Colorado, 112 p.

Campbell, S.D., M.W. Merritt, and J.T. DiStefano, 1989: Microburst recognition performance of TDWR operational testbed, *Third International Conference on the Aviation Weather System*, Anaheim, CA, AMS, Boston, Jan 30–Feb 3.

Caracena, F., P.M. Kuhn, and R.L. Kurkowski, 1981: Design and preliminary tests of an IR-airborne LLWS remote sensing system, *AIAA Paper 81–0239*, January.

Clough, S.A., *et al.*, 1986: Atmospheric radiance and transmittance: FASCODE 2, *Proceedings of 6th Conference on Atmospheric Radiation*, Williamsburg, VA, AMS, Boston, MA, 141–144.

Droegemeier, K.K. and M.R. Babcock, 1989: Numerical simulation of microburst downdrafts: application to on-board and look-ahead sensor technology, Preprints, *AIAA Aerospace Sciences Conference*, Reno, NV, Jan. 9–12.

Fawbush, E.J., and R.C. Miller, 1954: A basis for forecasting peak wind gusts in non-frontal thunderstorms, *Bull. Amer. Meteor. Soc.*, **35**, 14–19.

Federal Registry, 1988: Airborne low-altitude wind shear equipment and training requirements, Volume **53**, No. 187, Rules and Regulations, p. 37688. Department of Transportation, FAA, 14CFR Parts 121 and 135 [DOCET 19110: Ammendment Nos. 121–149, 135–27].

Foster, D.S., 1958: Thunderstorm gusts compared with computed downdraft speeds, *Mon. Wea. Rev.*, **86**, (3).

Fujita, T., 1985: The downburst, Department of Geophysical Sciences, University of Chicago, 122p.

Goff, C.R. and R.H. Gromzow, 1989: The Federal Aviation Administration's low level windshear alert system: a project management prospective, *Third International Conference on the Aviation Weather System*, Anaheim, CA, AMS, Boston, Jan 30–Feb 3.

Kneizys, F.X., *et al.*, 1988: Users Guide to LOWTRAN 7, Environmental Research Paper No. 1010, AFGL–TR–88–0177, Air Force Geophysics Lab., Hanscom AFB, MA.

Kuhn, P.M., R.L. Kurkowski, and F. Caracena, 1983: Airborne operation of an infrared low-level wind shear prediction system, *J. Aircraft*, **20**, 170–173.

Kuhn, P.M. and P.C. Sinclair, 1987: Airborne infrared wind shear detector performance in rain obscuration, *AIAA Paper, 25th Aerospace Conference*, Reno, NV, January.

National Research Council, 1983: Low altitude wind shear and its hazard to aviation. National Academy Press, Washington, D.C., 161 pp.

Mahoney, W., W. Wilson, K. Brishawn, and M.K. Poletovich, 1989: Microburst detection by TDWR: performance assessment, *Third International Conference on the Aviation Weather System*, Anaheim, CA, AMS, Boston, Jan 30–Feb 3.

McCarthy, J. and J.W. Wilson, 1985: The calssify, locate, and avoid wind shear (CLAWS) project at Denver's Stapleton International Airport: operational testing of terminal weather hazard warnings with an emphasis on microburst wind shear, Preprints, *2nd International Conference on the Aviation Weather System*, Montreal, Can., AMS, Boston, MA, 247–256.

Proctor, F.H., 1989: A relationship between peak temperature drag and velocity differential in a microburst, *Third International Conference on the Aviation Weather System*, Anaheim, CA, AMS, Boston, Jan 30–Feb 3.

Research Applications Program, 1988: Terminal doppler weather radar (TDWR): a briefing paper, Prepared for the Federal Aviation Administration by the Research Applications Program, National Center for Atmospheric Research, Boulder, CO.

Sinclair, P.C., 1973: Severe storm air velocity and temperature structure deduced from penetrating aircraft. *Preprints, 8th Conference on Severe Local Storms*. AMS, Boston, MA, Oct. 15–17.

Sinclair, P.C., 1979: Velocity and temperature structure near and within severe storms. *Preprints, 11th Conference on Severe Local Storms*, AMS, Boston, MA, Oct. 2–5.

Sinclair, P.C. and J.F.W. Purdom, 1983a: The genesis and development of deep convective storms, Final Report, NOAA Grant NA80AA-D-00056, CIRA, Colorado State University, Fort Collins, January.

Sinclair, P.C. and J.F.W. Purdom, 1983b: Shuttle recovery requirements and the development of arc cloud lines from the thunderstorm outflows, *Preprints, 9th Conference on Aerospace and Aeronautical Meteorology*, AMS, Boston, MA, June 6–9.

Sinclair, P.C. and J.F.W. Purdom, 1984: Aircraft penetrations of arc cloud lines, *Preprints, Conference on Sattellite/Remote Sensing and Applications*, AMS, Boston, MA, June 25–29.

Sinclair, P.C. and P.M. Kuhn, 1987: Forward looking airborne infrared wind shear sensor operation in precipitation. Final Report to NOAA, Environmental Research Laboratory, Boulder, CO, September.

Sinclair, P.C. and J.F.W. Purdom, 1989: Real-time data acquisition and interactive display system for a small, single-engine, atmospheric research aircraft. Submitted to *J. Atmos. Oceanic Tech.*

Sinclair, P.C. and P.M. Kuhn, 1989: Aircraft low level wind shear detection and warning system, *Third International Conference on the Aviation Weather System*, Anaheim, CA, AMS, Boston, Jan 30–Feb 3.

Smythe, G.R., 1989: Evaluation of the 12-station enhanced low level wind shear alert system (LLWS) at Denver Stapleton International Airport, *Third International Conference on the Aviation Weather System*, Anaheim, CA, AMS, Boston, Jan 30–Feb 3.

Stengel, R.F., 1984: Unsolved issues in wind shear encounters, NASA Conf. Publication, 2474: *Wind Shear/Turbulence Inputs to Flight Simulation and Systems Certification.* Langley Research Center, Hampton, VA, May 30-June 1.

Targ, R. and R.L. Bowles, 1988: Investigation of airborne lidar for avoidance of wind shear hazards, Preprints, *2nd Combined Maunfacturer's and Technology Airborne Windshear Review Meeting*, Williamsburg, VA, October 18–20.

Turnbull, D., J. McCarthy, J. Evans, and D. Zrnic, 1989: The FAA terminal doppler weather radar (TDWR) program, *Third International Conference on the Aviation Weather System*, Anaheim, CA, AMS, Boston, Jan 30–Feb 3.

Wilson, F.W., Jr., and J.A. Flueck, 1986: A study of the methodology of low altitude wind shear detection with special emphasis on the low level wind shear alert system concept, Final Report, DOT/FAA/PM–86/4. DOT/FAA, Program Engineering Maintenance Service, Washington, D.C., 101 pp. (Available through NTIS, Springfield, VA 22161).

Figure Captions

Fig. 1 LAWS/MB Detection Systems. R_L and R_T refer to reactive systems that require the aircraft to penetrate and react to the LAWS/MB circulation. Surface based single doppler radars (TDWR) have good surveilance capabilities but may not detect all MB's (dry) or winds at low altitudes. The FLIR system remotely monitors the cold downdraft region of the MB during landing and takeoff. Vertical scanning avoids intercept with ground surface and warm boundary layer air.

Fig. 2 Thunderstorm Microburst Detection by Scanning FLIR System. The forward scanning and ranging capabilities of the new FLIR system provides a 50–70 second warning of microburst penetration to the pilot of the approaching aircraft. Note that the FLIR system has an IFOV that intercepts the MB in a horizontal plane above the ground surface.

Fig. 3 Wing-mounted Forward-Looking Radiometer Pod. The radiometer FOV($\pm 10°$) is completely outside of the engine propellor arc. The radiometric measurements are supplemented with:

- Gust probe measurements of u', v', w'.
- Doppler (navigation) wind measurements of $\bar{u}, \bar{v}$.
- Temperature and dewpoint measurements.
- Real-Time, Computer (MASSCOMP/Concurrent Systems) controlled data acquisition, data storage, and color graphical display.

Fig. 4 Relationship of Thunderstorm Peak Gust with Temperature Drop (ΔT) at the Surface (Fawbush and Miller, 1954).

Fig. 5 Transmittance of a 1,000–foot path in air at sea level containing 5.7 millimeters of precipitable water at a temperature of 79°F.

Fig. 6 CO_2 weighting functions for passbands 20 cm^{-1} wide about center frequencies labeled in the figure.

Fig. 7 Mid-Level Penetration of Wet Microburst with T207 Research Aircraft.

Fig. 8 MB#1; Variations of Vertical Motion (w), Horizontal Winds (V_H), Temperature (T_s), and Radiometric Temperature Difference (ΔT_R) During a Wet Microburst Penetration (see text for explanation and discussion).

Fig. 9 MB#1 Cross-Section of Flight Paths and Vertical Motion Field (w) With Respect to Distance (x) in km from the Initial Point at $z \approx 550$ m. The mean (layer) environmental wind [$V_H(c)$] and the MB translation velocity at mid-levels is labeled along with the depiction of heavy (HP) and Light (LP) precipitation. The lower graph shows the variability of the hazard factors F and F^* along the flight path (see text for further explanation).

Fig. 10 MB#2 Variations of Vertical Motion (w), Horizontal Winds (V_H), Temperature (T_s), and Radiometric Temperature Difference (ΔT) During a Wet Microburst Penetration (see text for explanation and discussion).

Fig. 11 MB#2; See Figure 9 and text for explanation.

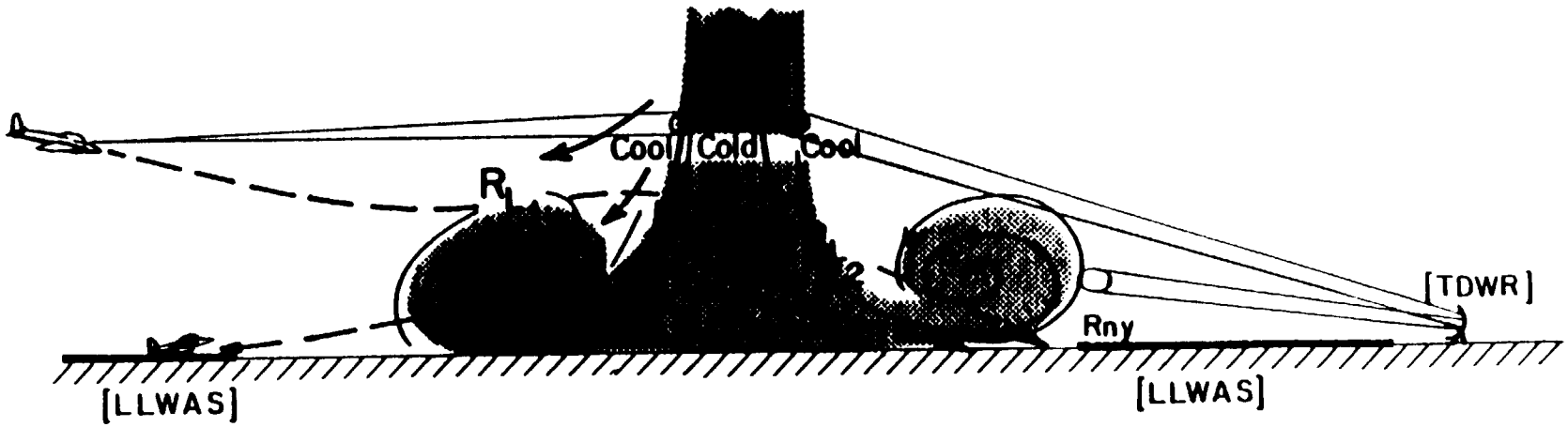
Cool
Cold
Cool
R1
R2
[TDWR]
Rny
[LLWAS]
[LLWAS]

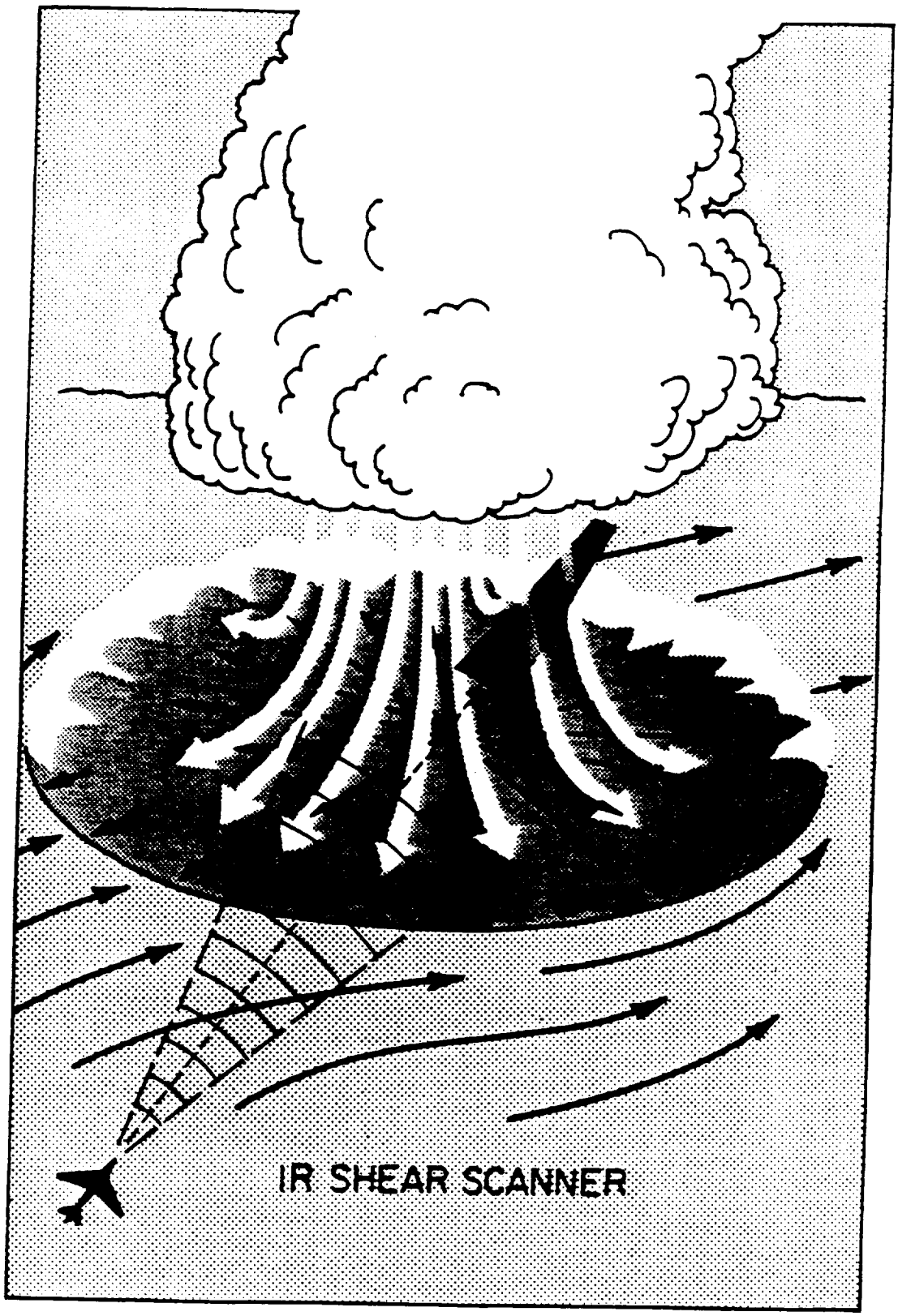
IR SHEAR SCANNER

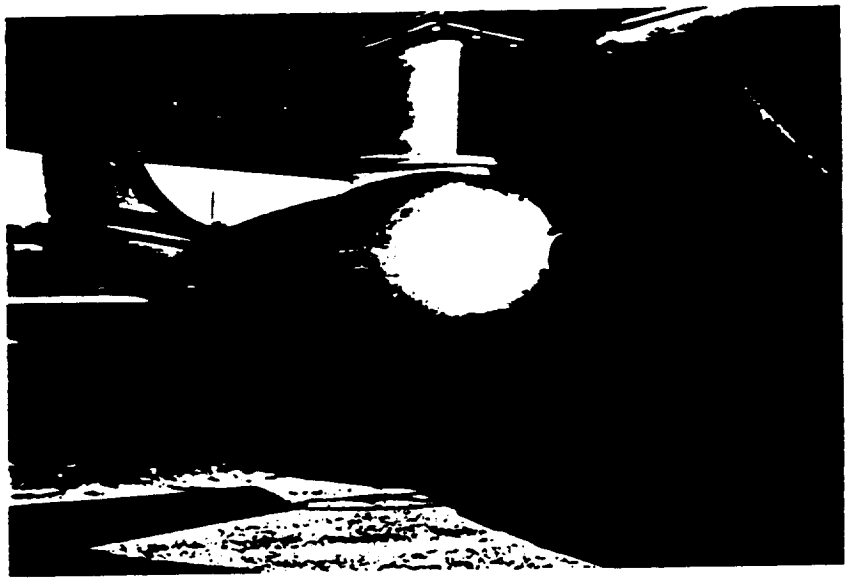

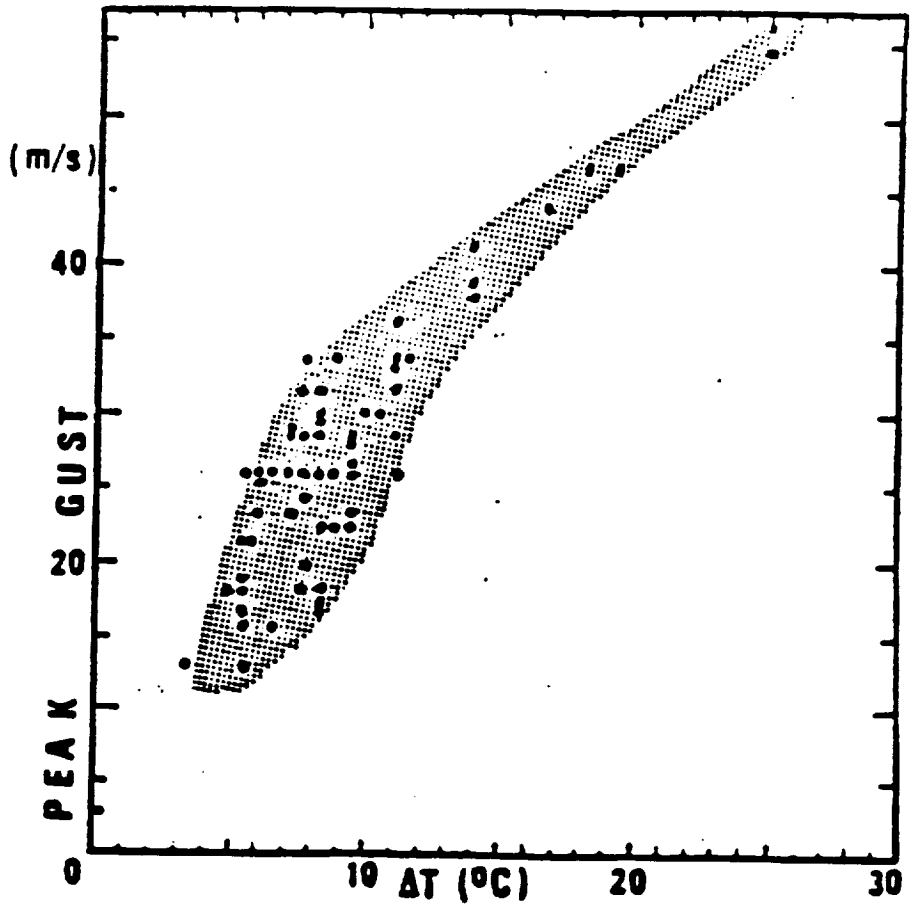
(m/s)
40
20
0
PEAK GUST
10
ΔT (°C)
20
30

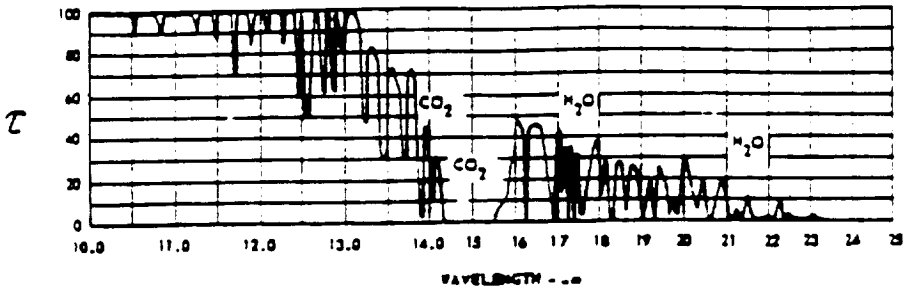
τ
100
80
60
40
20
0
CO_2
CO_2
H_2O
H_2O
10.0
11.0
12.0
13.0
14.0
15
16
17
18
19
20
21
22
23
24
25

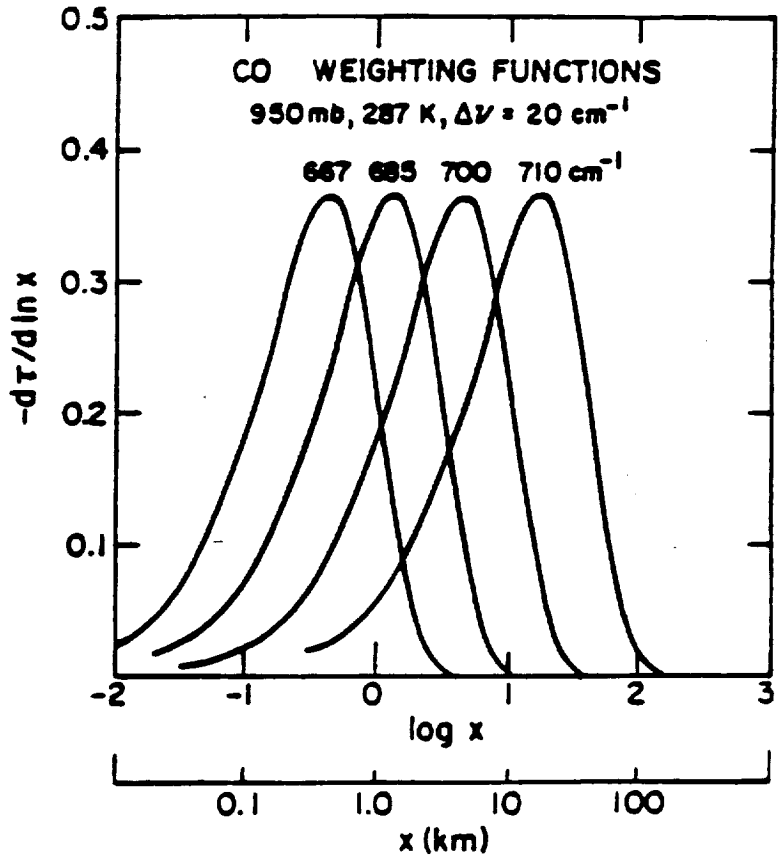
CO WEIGHTING FUNCTIONS
950 mb, 287 K, Δν = 20 cm⁻¹
667 685 700 710 cm⁻¹
-dτ/d ln x
0.5
0.4
0.3
0.2
0.1
-2
-1
0
1
2
3
log x
0.1
1.0
10
100
x (km)

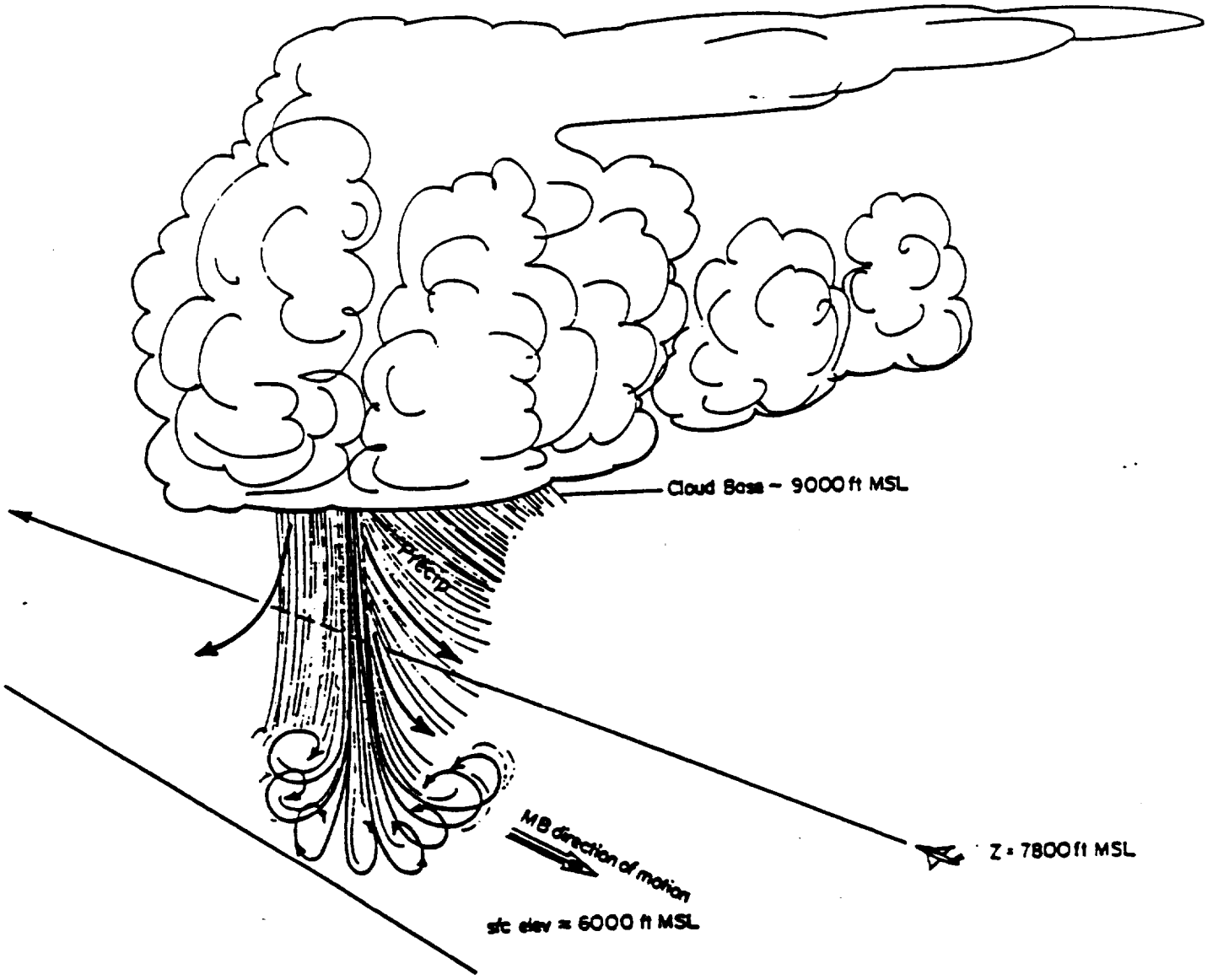
Cloud Base ~ 9000 ft MSL
Precip
MB direction of motion
Z = 7800 ft MSL
stc elev = 6000 ft MSL

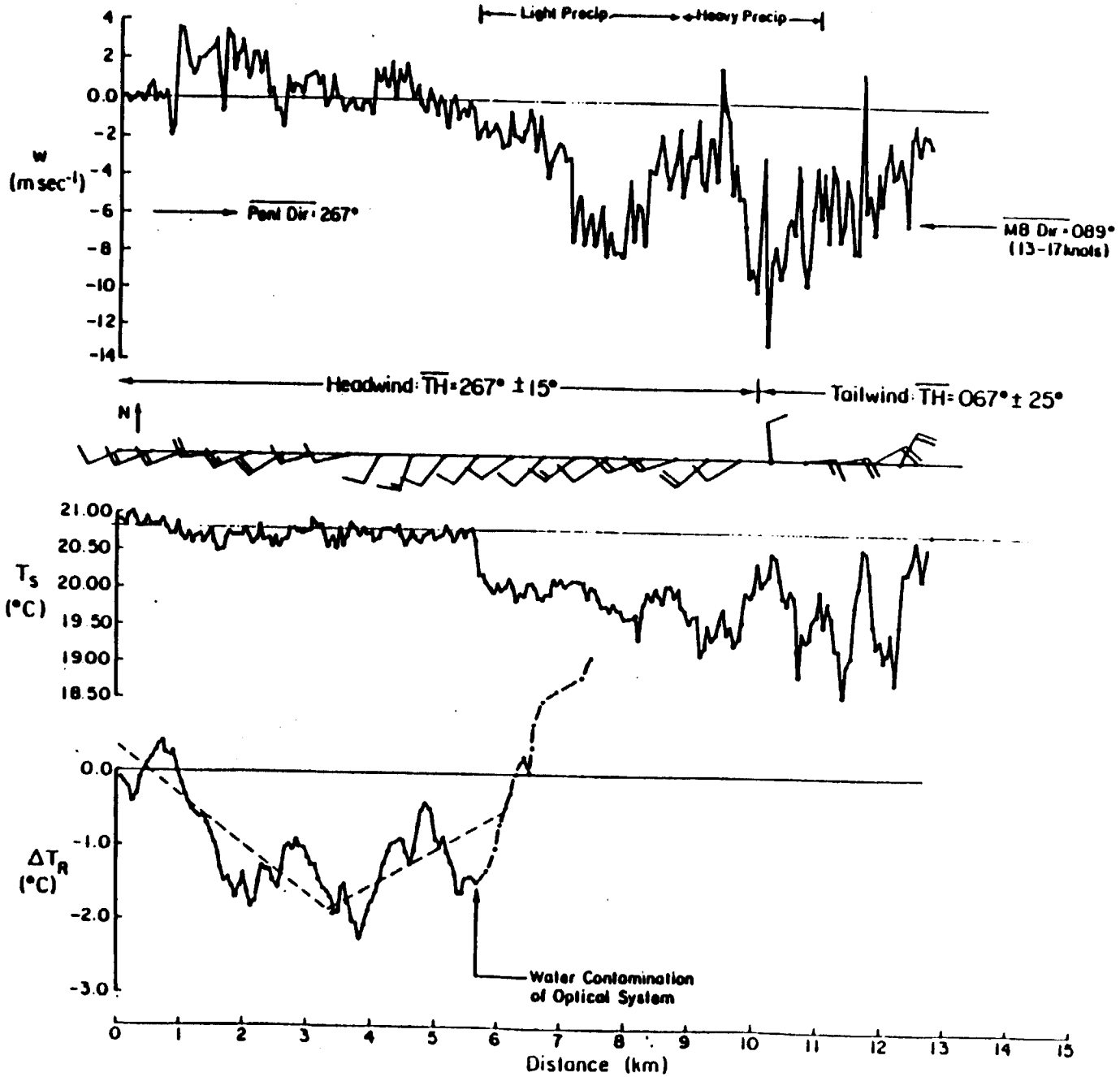
Light Precip
Heavy Precip
w (m sec⁻¹)
4
2
0.0
-2
-4
-6
-8
-10
-12
-14
Pent Dir: 267°
M8 Dir: 089°
(13-17 knots)
Headwind: TH=267° ± 15°
Tailwind: TH= 067° ± 25°
N
Ts (°C)
21.00
20.50
20.00
19.50
19.00
18.50
ΔTR (°C)
0.0
-1.0
-2.0
-3.0
Water Contamination of Optical System
0
1
2
3
4
5
6
7
8
9
10
11
12
13
14
15
Distance (km)

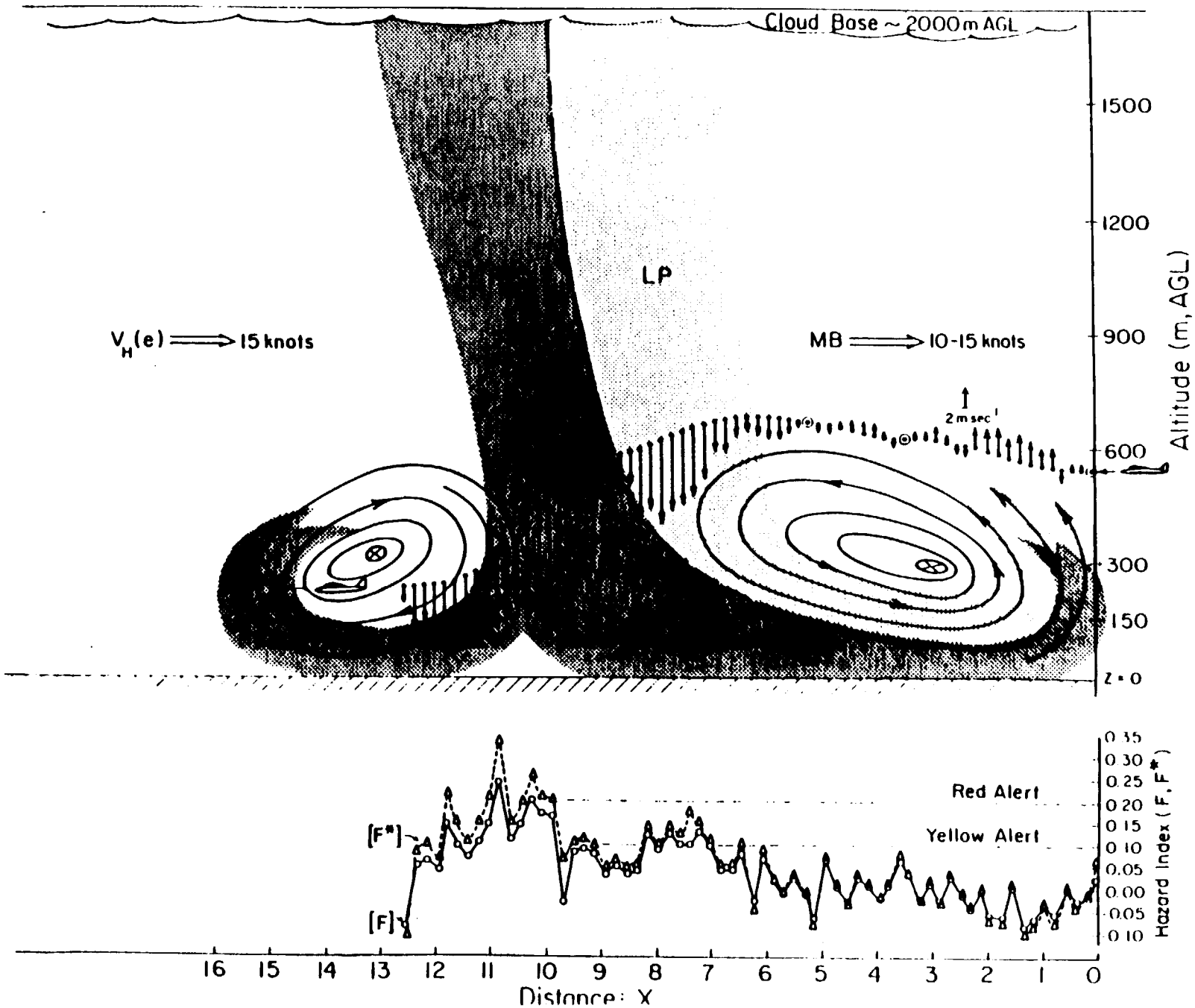
Cloud Base ~ 2000 m AGL
LP
$V_H(e)$ ⟹ 15 knots
MB ⟹ 10-15 knots
2 m sec⁻¹
1500
1200
900
600
300
150
z = 0
Altitude (m, AGL)
[F*]
[F]
Red Alert
Yellow Alert
0.35
0.30
0.25
0.20
0.15
0.10
0.05
0.00
-0.05
-0.10
Hazard Index (F, F*)
16 15 14 13 12 11 10 9 8 7 6 5 4 3 2 1 0
Distance: X

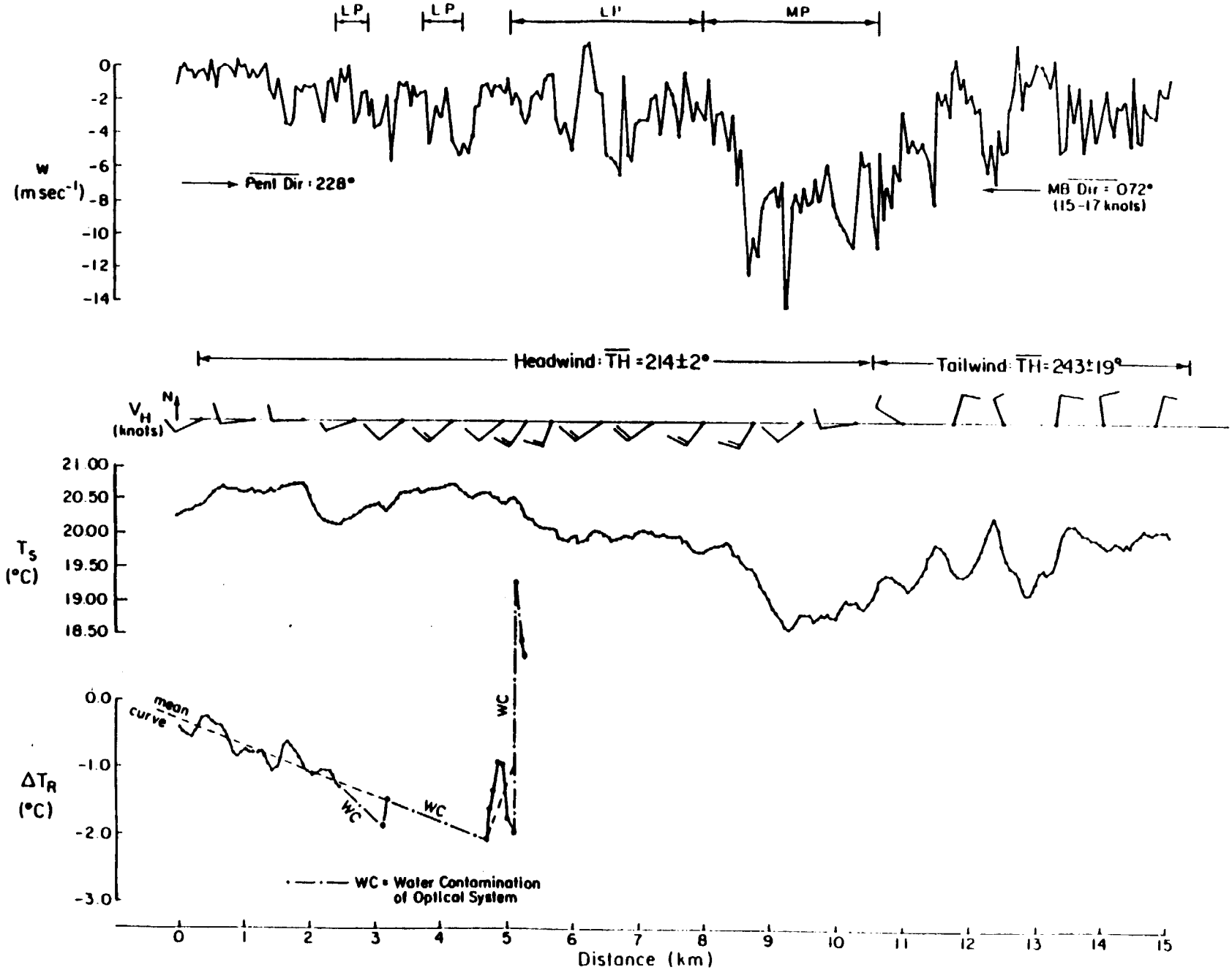
LP
LP
LP
MP
w (m sec⁻¹)
0
-2
-4
-6
-8
-10
-12
-14
Penl Dir : 228°
MB Dir = 072°
(15-17 knots)
Headwind: TH = 214±2°
Tailwind: TH = 243±19°
V_H (knots)
N
T_S (°C)
21.00
20.50
20.00
19.50
19.00
18.50
ΔT_R (°C)
0.0
-1.0
-2.0
-3.0
mean curve
WC
WC
WC
WC = Water Contamination of Optical System
0
1
2
3
4
5
6
7
8
9
10
11
12
13
14
15
Distance (km)

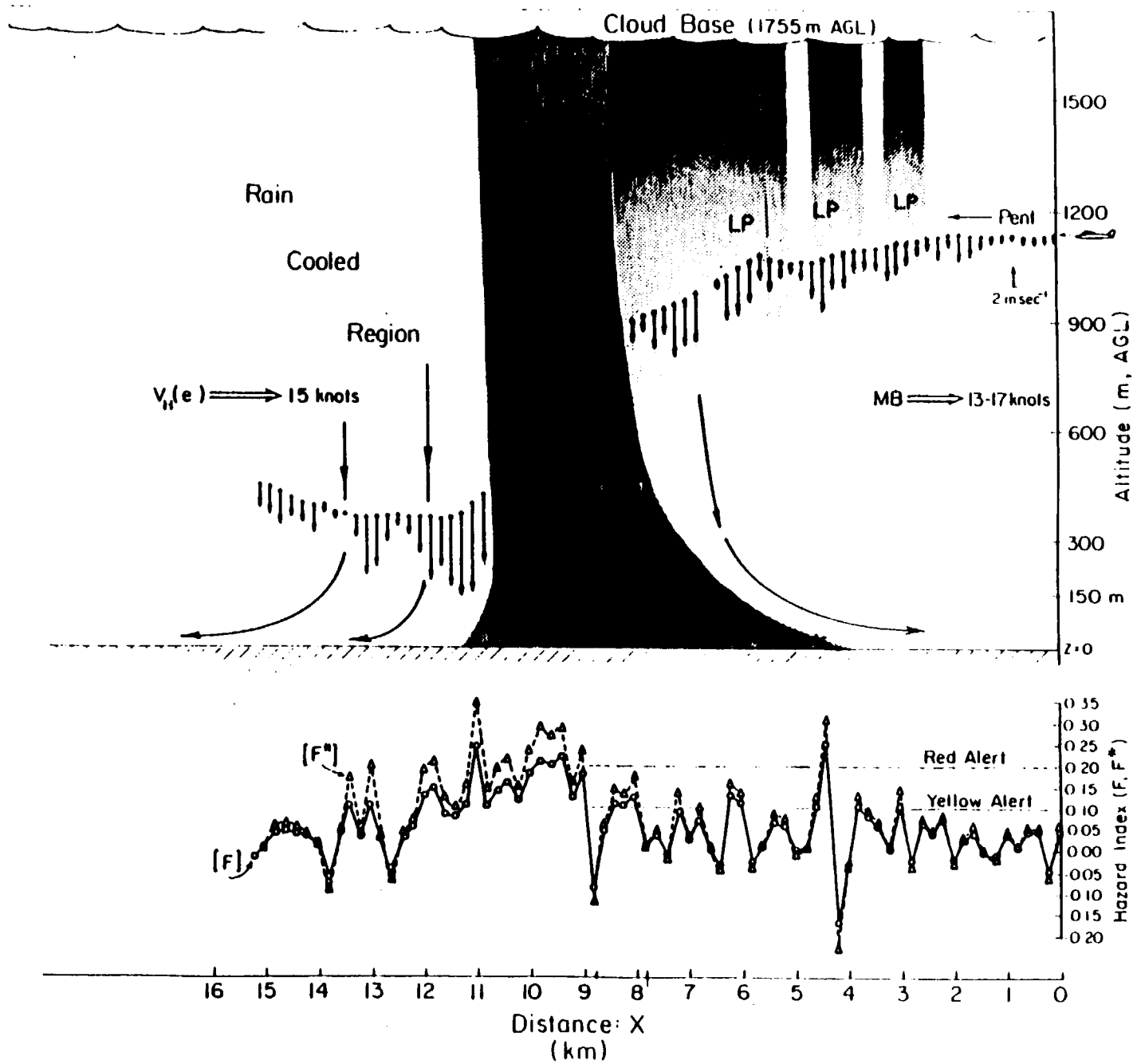
Cloud Base (1755 m AGL)
Rain
Cooled
Region
LP
LP
LP
Pent
2 m sec⁻¹
V_{tt}(e) ⟹ 15 knots
MB ⟹ 13-17 knots
1500
1200
900
600
300
150 m
Z=0
Altitude (m, AGL)
[F*]
[F]
Red Alert
Yellow Alert
0.35
0.30
0.25
0.20
0.15
0.10
0.05
0.00
-.05
-.10
-.15
-.20
Hazard Index (F, F*)
16 15 14 13 12 11 10 9 8 7 6 5 4 3 2 1 0
Distance: X
(km)

Status of Colorado State Universities' IR Research
Questions and Answers

Q: DAVE HINTON (NASA Langley) - You discussed a microburst penetration technique for your Cessna that involved lowering the nose to increase or preserve airspeed, then trailing off this airspeed for potential energy at low altitude. I can understand doing this during intentional research penetrations begun at reasonable altitudes, but I am skeptical that this could be safely performed in an inverted encounter at low altitude, say 100 or 200 feet AGL. Are you advocating a pitch down technique for general aviation pilots?

A: PETE SINCLAIR (Colorado Stare University) - Yes. For intense microbursts with down-drafts of greater than 7 to 10 meters per second. The amount of pitch down, of course, will depend on the magnitude of the down-draft and the altitude above ground level.

Q: DAVE HINTON (NASA Langley) - Have you conducted any piloted simulation studies to determine the acceptability and viability of this procedure for GA pilots of average skill?

A: PETE SINCLAIR (Colorado Stare University) - Not yet, but I plan to enter our measured wind profiles into a flight simulator for development of GA flight procedures.

ROLAND BOWLES (NASA Langley) - It amazes me that people don't understand that you descend when you lower the nose of an airplane. It also surprises me that we talk about airspeed loss, dynamic pressure, forces on big lifting surfaces of 20 to 30% and realize that there is still the factors of 2 in lift coefficient by just getting the wing bite into the relative wind in the right way. It's not a very simple problem.

WAYNE SAND (NCAR) - I guess I have to respond a little bit. There is some foundation to what Peter is saying in this whole thing. It's a technique that actually has been proven by the sail plane people. They do this all the time to deal with rotor clouds when they're doing wave flights and all that sort of thing. The way they deal with it, to get through there as quickly as possible with the least altitude loss possible, is to go fast and to get the nose down. So I think that's the foundation for a lot of what he's saying and what he's trying to suggest. I think it's a long ways from proving that's the right way to do it. One of our people has gone through some calculations on that with this sort of thing in mind and actually came up with the same conclusion that you're probably better off in a light plane to get through there as quickly as you can however you do that, providing you have the ground clearance and all that sort of thing. I'm certainly not to the point of advocating that yet either. It is something to think about and it's one of the points that I think should be addressed.

ROLAND BOWLES (NASA Langley) - Sail planes don't have engines on them. One of the first rules is to get the thrust above the horizon.

UNKNOWN - Being both a sail plane pilot and a general aviation commercial sector pilot, I was just going to emphasize that in the sail plane arena the only option he's got to increase his forward speed, and therefore minimize the time in the shear, is by lowering his nose. That's the reason why we do that. However, in our sector, particularly the commercial sector, you have other options available. I think that Peter's goal is certainly worthwhile and that's to minimize the time in the shear. I think we can all agree that's a worthwhile objective but whether you lower the nose and go for the ground in order to do that or not is probably worth discussing.

DAVE HINTON (NASA Langley) - I'm also a sail plane pilot and I also understand wanting to put the nose down to get out of the sink as quickly as you can. But what works at 3000 feet may not work at 30. As anybody that has done any research on recovery procedures knows, you can't simply go for the optimal recovery technique and say fly it, there are other factors involved.

Session X. Airborne Doppler Radar / Industry